

1  
2 **Controls on Ice Cliff Formation, Distribution and Characteristics on Debris-Covered**  
3 **Glaciers**

4 **M. Kneib<sup>1,2</sup>, Catriona Fyffe<sup>3</sup>, Evan S. Miles<sup>1</sup>, Shayna Lindemann<sup>1</sup>, Thomas E. Shaw<sup>1</sup>,**  
5 **Pascal Buri<sup>1</sup>, Michael McCarthy<sup>1</sup>, Boris Ouvry<sup>4</sup>, Andreas Vieli<sup>4</sup>, Yota Sato<sup>5</sup>, Philip D.A**  
6 **Kraaijenbrink<sup>6</sup>, Chuanxi Zhao<sup>7,8</sup>, Peter Molnar<sup>2</sup>, Francesca Pellicciotti<sup>1,3</sup>**

7 <sup>1</sup> High Mountain Glaciers and Hydrology Group, Swiss Federal Institute, WSL, Birmensdorf,  
8 Switzerland.

9 <sup>2</sup> Institute of Environmental Engineering, ETH Zürich, Zürich, Switzerland

10 <sup>3</sup> Department of Geography and Environmental Sciences, Northumbria University, Newcastle  
11 upon Tyne, UK

12 <sup>4</sup> Department of Geography, University of Zurich, 8057 Zurich, Switzerland

13 <sup>5</sup> Graduate School of Environmental Studies, Nagoya University, Nagoya, Japan

14 <sup>6</sup> Utrecht University, Department of Physical Geography, PO Box 80115, 3508 TC, Utrecht, The  
15 Netherlands.

16 <sup>7</sup> College of Earth and Environmental Sciences, Lanzhou University, Lanzhou 730000, China

17 <sup>8</sup> State Key Laboratory of Tibetan Plateau Earth System, Environment and Resources (TPESER),  
18 Institute of Tibetan Plateau Research, Chinese Academy of Sciences

19  
20 Corresponding author: Marin Kneib ([marin.kneib@gmail.com](mailto:marin.kneib@gmail.com))

21 **Key Points:**

- 22 • We derived an unprecedented dataset of 37537 ice cliffs and their characteristics across  
23 86 debris-covered glaciers in High Mountain Asia
- 24 • We find that 38.9% of the cliffs are stream-influenced, 19.5% pond-influenced and  
25 19.7% are crevasses
- 26 • Ice cliff distribution can be predicted by velocity as an indicator of both the dynamics and  
27 state of evolution of debris-covered glaciers  
28

29 **Abstract**

30

31 Ice cliff distribution plays a major role in determining the melt of debris-covered glaciers but its  
32 controls are largely unknown. We assembled a dataset of 37537 ice cliffs and determined their  
33 characteristics across 86 debris-covered glaciers within High Mountain Asia (HMA). We  
34 complemented this dataset with the analysis of 202 cliff formation events from multi-temporal  
35 UAV observations for a subset of glaciers. We find that 38.9% of the cliffs are stream-  
36 influenced, 19.5% pond-influenced and 19.7% are crevasses. Surface velocity is the main  
37 predictor of cliff distribution at both local and glacier scale, indicating its dependence on the  
38 dynamic state and hence evolution stage of debris-covered glacier tongues. Supraglacial ponds  
39 contribute to maintaining cliffs in areas of thicker debris, but this is only possible if water  
40 accumulates at the surface. Overall, total cliff density decreases exponentially with debris  
41 thickness as soon as debris gets thicker than 10 cm.

42

43 **Plain Language Summary**

44

45 Debris-covered glaciers are common throughout the world's mountain ranges and are  
46 characterised by the presence of steep ice cliffs among the debris-covered ice. It is well-known  
47 that the cliffs are responsible for a large portion of the melt of these glaciers but the way they  
48 form, and as a result the controls on their development and distribution across glaciers remains  
49 poorly understood. Novel mapping approaches combined with high-resolution satellite and drone  
50 products enabled us to disentangle some of these controls and to show that the ice cliffs are  
51 generally formed and maintained by the surface hydrology (ponds or streams) or by the opening  
52 of crevasses. As a result, they depend both at the local and glacier scale on the dynamic state of

53 the glaciers as well as the evolution stage of their debris cover. This provides a pathway to better  
54 represent their contribution to glacier melt in predictive glacier models.

55

## 56 **1 Introduction**

57 Debris-covered glaciers are found in all mountain ranges (Scherler et al., 2018), and  
58 supraglacial debris extents and thickness are expected to increase in a warming climate  
59 (Compagno et al., 2022; Herreid & Pellicciotti, 2020; Stokes et al., 2007). However, despite  
60 considerable recent advances, modelling the mass balances of these glaciers remains challenging  
61 (Rounce et al., 2021). This is partly due to the presence of supraglacial ice cliffs, which melt up  
62 to 20 times faster than the surrounding debris-covered ice, therefore compensating for the  
63 relatively well constrained debris insulating effect (Anderson, Armstrong, Anderson, & Buri,  
64 2021; Brun et al., 2018; E. S. Miles, Willis, et al., 2018; Reid & Brock, 2014; Sakai et al., 1998,  
65 2002). In one catchment in High Mountain Asia (HMA) ice cliffs were shown to contribute 17+/-  
66 4% of the melt of the debris-covered ice (Buri et al., 2021). This has major implications for the  
67 mass balance of debris-covered glaciers (Pellicciotti et al., 2015) and their long-term evolution  
68 (Ferguson & Vieli, 2021; Racoviteanu et al., 2022).

69

70 While models accurately simulate the energy and mass balance contribution of individual  
71 ice cliffs (Buri et al., 2016; Kneib et al., 2022), their application at large spatial scales is limited  
72 by our understanding of the controls of ice cliff distribution. Indeed, estimates of ice cliff density  
73 are difficult to make (Anderson, Armstrong, Anderson, & Buri, 2021; Herreid & Pellicciotti,  
74 2018; Kneib et al., 2020) and vary widely in time and space, between 1 and 15% of the debris-  
75 covered area (e.g. Falaschi et al., 2021; Kneib et al., 2021; Loriaux & Ruiz, 2021; Sato et al.,  
76 2021; Steiner et al., 2019; Watson et al., 2017). Remote sensing studies have shown that cliffs  
77 are often associated with ponds (Steiner et al., 2019; Watson, Quincey, Carrivick, et al., 2017),  
78 hinting at a preferential location of ice cliffs where lower glacier longitudinal gradient and  
79 surface velocities promote surface ponding (Bolch et al., 2008; Quincey et al., 2007; Quincey &  
80 Glasser, 2009; Racoviteanu et al., 2021; Reynolds, 2000; Sakai & Fujita, 2010; Salerno et al.,  
81 2012). Other limited observations indicate that ice cliffs preferentially develop at the confluence

82 of glacial tributaries, in locations of high compressive strain rates, and areas of thinner debris  
83 (Anderson, Armstrong, Anderson, & Buri, 2021; Anderson, Armstrong, Anderson, Scherler, et  
84 al., 2021; Benn et al., 2012; Kraaijenbrink et al., 2016; Steiner et al., 2019; Watson, Quincey,  
85 Carrivick, et al., 2017). However, the lack of consistent observations of cliff distribution makes it  
86 difficult to include ice cliffs in predictive glacier models in a way that accounts for their spatial  
87 distribution and temporal evolution.

88

89 Ice cliff survival is inherently linked to debris stability, which is a function of local slope,  
90 debris thickness and water content, as well as undercutting by streams or ponds (Moore, 2018).  
91 The local slope can change in relatively short time scales with differential melt caused by  
92 heterogeneous debris thicknesses (Moore, 2021; Nicholson et al., 2018; Sharp, 1949), which  
93 results in the surface of debris-covered glaciers being particularly hummocky where the debris  
94 gets thicker than 20-30 cm (Bartlett et al., 2020; King et al., 2020). Slope undercutting and  
95 destabilisation by streams or ponds is expected to be one of the main triggers for ice cliff  
96 formation (Mölg et al., 2019; Röhl, 2006, 2008; Sakai & Takeuchi, 2000) and survival (Benn et  
97 al., 2001, 2012; Brun et al., 2016; Kneib et al., 2022; Sato et al., 2021; Watson, Quincey, Smith,  
98 et al., 2017). Other hypothesised cliff formation mechanisms include crevasse opening (Reid &  
99 Brock, 2014; Steiner et al., 2019) or the collapse of englacial conduits (Egli et al., 2021; Gulley  
100 et al., 2009; Immerzeel et al., 2014; E. S. Miles, Watson, et al., 2018; K. E. Miles et al., 2020;  
101 Sakai & Takeuchi, 2000), but these hypotheses have never been tested in a quantitative way.

102

103 In this study, we therefore 1) map ice cliffs across 86 glaciers in HMA, 2) determine their  
104 physical characteristics, 3) attribute their distribution to potential local and glacier-wide  
105 controlling factors. The findings are further corroborated by complementary observations on ice  
106 cliff formation from high-resolution, multi-temporal Unoccupied Aerial Vehicle (UAV) data at  
107 five of the studied glaciers (Text S1).

108

## 109 **2 Data and Methods**

110

111 We used 14 Pléiades stereo-images acquired between 2017 and 2021 to derive 2m-  
112 resolution multi-spectral images and Digital Elevation Models (DEMs) covering 86 debris-  
113 covered glaciers across HMA (Berthier et al., 2014; Shean et al., 2016; Fig. 1; Table S2), 70 of  
114 which had more than 65% of their debris-covered area that could be classified after removal of  
115 clouds, shadows and fresh-snow (Table S3). The DEMs were used to derive surface slope and  
116 aspect, the glacier ‘hummockiness’, which we defined as the percentage of area for which the  
117 Statistical Measure of Relief (SMR) calculated over a 8 m window was greater than 50 m (King  
118 et al., 2020), as well as supraglacial channels (Schwanghart & Scherler, 2014; Text S2). The  
119 multi-spectral images were used to manually update the glacier and debris outlines of the RGI  
120 6.0 (Pfeffer et al., 2014; Scherler et al., 2018; Table S3). Glacier longitudinal gradient was  
121 computed using the 30m resolution AW3D DEM (Dehecq et al., 2019; Tadono et al., 2014) and  
122 combined with glacier ice thicknesses (Farinotti et al., 2019) to estimate driving stress over a  
123 distance of two ice thicknesses. Distributed glacier velocity, compressive and tensile strain rates  
124 were obtained from the global 50m resolution composite by Millan et al. (2022). We additionally  
125 used the distributed debris thickness dataset of McCarthy et al. (2022) for all glaciers larger than  
126 2 km<sup>2</sup> (64 glaciers, 47 of which have more than 65% of their debris-covered area that could be  
127 classified). All these datasets were aggregated 1) in 500 m distance bins along the glacier  
128 flowlines (Kienholz et al., 2014; King et al., 2020) and 2) for each glacier. Data gaps within the  
129 bins were filled using a nearest neighbour interpolation.

130

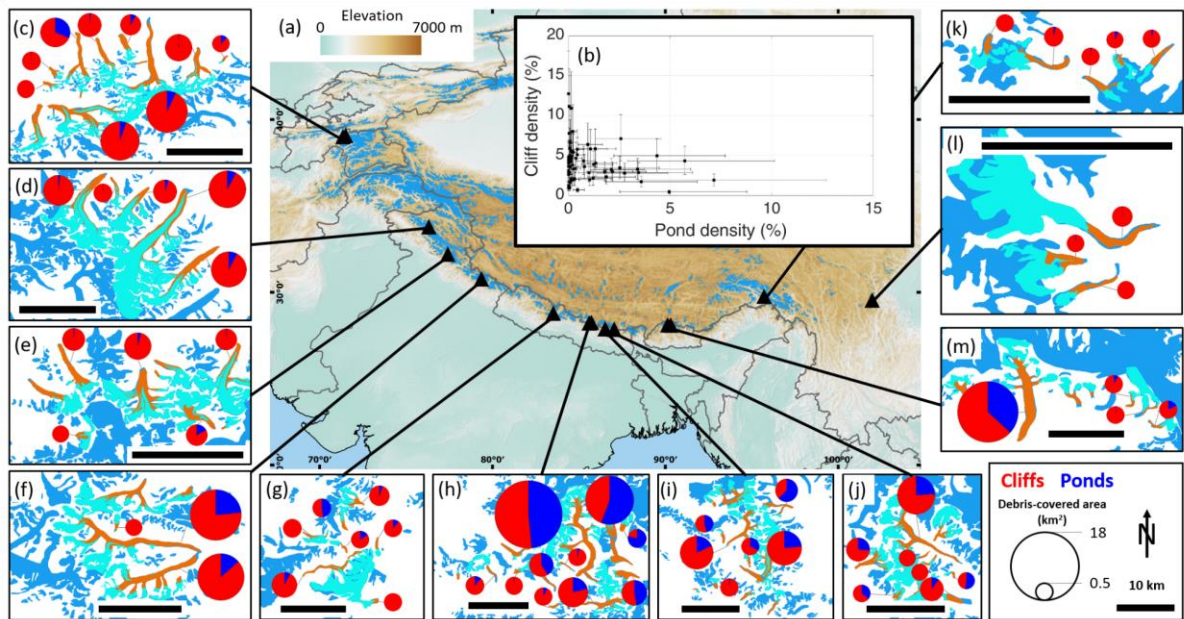
131 Ice cliffs and ponds were derived automatically in each Pléiades scene following the  
132 Spectral Curvature method for cliffs, which is based solely on spectral characteristics (Kneib et  
133 al., 2020), and the Normalized Difference Water Index (NDWI) for ponds (McFeeters, 1996; E.  
134 S. Miles et al., 2017; Watson et al., 2016, 2018; Text S2). The ice cliffs are then implicitly  
135 defined here as exposed ice in an otherwise debris-covered domain, therefore likely to undergo  
136 ‘enhanced’ melt locally. Some of these features were clearly identifiable as crevasses due to their  
137 elongated, straight or slightly curved shapes and these zones were outlined manually. Past

138 studies have only examined high-relief (several meters) ice cliffs, but here our interest is in all  
 139 exposed ice in the debris-covered area, so we include smaller features common for thin-debris  
 140 areas, such as crevasses, which similarly enhance surface ablation (Colgan et al., 2016).

141

142 Multi-temporal UAV data with a monitoring period longer than 2 years and with at least  
 143 3 high-resolution (<1 m) DEMs and orthoimages were available at five of the studied glaciers  
 144 distributed across HMA. This complementary data was used to identify ice cliff formation events  
 145 and derive the characteristics of newly formed ice cliffs (Text S1).

146



147 **Figure 1:** (a) Map of HMA with each triangle representing one of the 14 Pléiades scenes  
 148 (some scenes are very close to each other) and the boxes to the side (c-m) showing a zoomed  
 149 view of the glaciers in these areas. The background is the GTOPO 30 arc seconds (~1 km) DEM,  
 150 and the glacierised areas are indicated in blue. The inset boxes show the glacier RGI 6.0  
 151 outlines in dark blue, the glaciers visible in the Pléiades images in turquoise and their debris-  
 152 covered areas in brown. The pie charts are scaled to the absolute size of the debris-covered  
 153 areas and show the relative proportion of ponds (dark blue) and cliffs (red) for each glacier for

154 *which more than 65% of their debris-covered area could be classified. (b) Cliff and pond density*  
155 *of each of these glaciers. The bars show the uncertainties.*

156

## 157 **3 Results**

### 158 **3.1. Influence of supraglacial hydrology on ice cliff distribution**

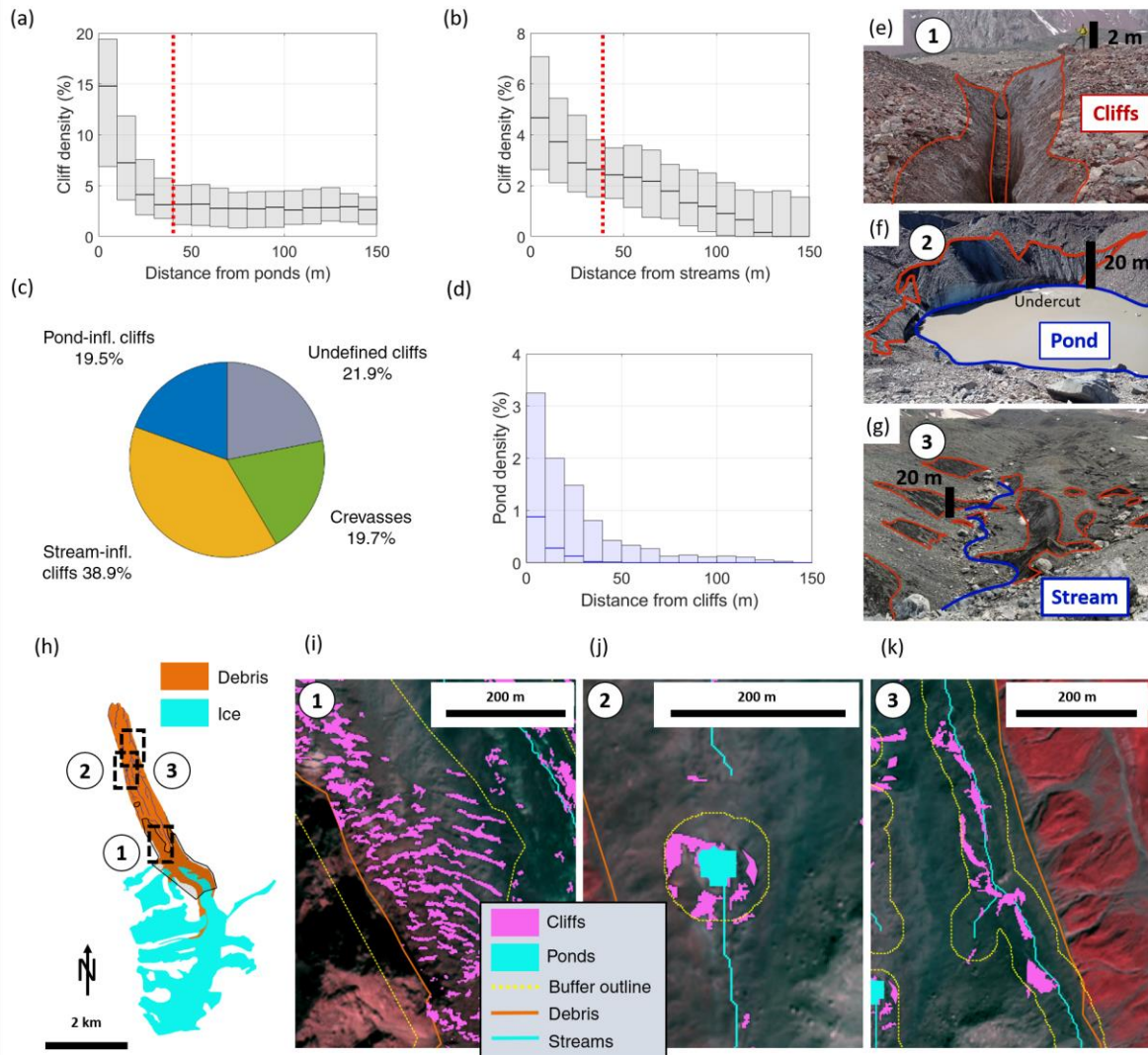
159

160 Cliffs are preferentially located in the vicinity of ponds and streams, as their density  
161 strongly decreases with distance from these hydrological features (Fig. 2a, b), and a large  
162 majority of the ponds are related to at least one neighbouring cliff (Fig. 2d). This is further  
163 confirmed by field observations (Fig. 2e-g) and multitemporal UAV observations showing that  
164 the presence of streams or ponds is responsible for more than 79% of the newly-formed cliff area  
165 (Fig. S2). This leads us to define a 40m-buffer around ponds and streams within which we  
166 classify the cliff pixels as pond-influenced or stream-influenced (Fig. 2h). With this definition,  
167 pond-influenced cliffs account for 19.5% and stream-influenced cliffs for 38.9% of the total cliff  
168 area (Fig. 2c). In addition, crevasses represent 19.7% of the cliff area across all glaciers. They  
169 are mostly located in the upper extents of the debris-covered areas but also appear lower down  
170 glacier, at shear margins, and in the vicinity of proglacial lakes or lateral streams entering the  
171 glacier (Fig. S6). The remaining cliffs are qualified as undefined. The stream mapping  
172 parameters and choice of buffer size have little influence on this classification (Fig. 2h, S12).

173

174 The slope and density of ice cliffs vary between categories, while this is less the case for  
175 aspect and size (Fig. S13). Crevasses are usually more densely distributed (15.2% of buffer area),  
176 followed by the pond-influenced (6.7%), stream-influenced (4.3%) and undefined cliffs (2.1% of  
177 remaining area, Fig. S13a). Despite a variety of glacier aspects (Table S3), there is a clear  
178 preferential cliff aspect distribution in the NNW direction for all categories (Fig. S13d), while  
179 the newly formed cliffs do not appear to have a preferential aspect (Sato et al., 2021; Fig. S4).

180



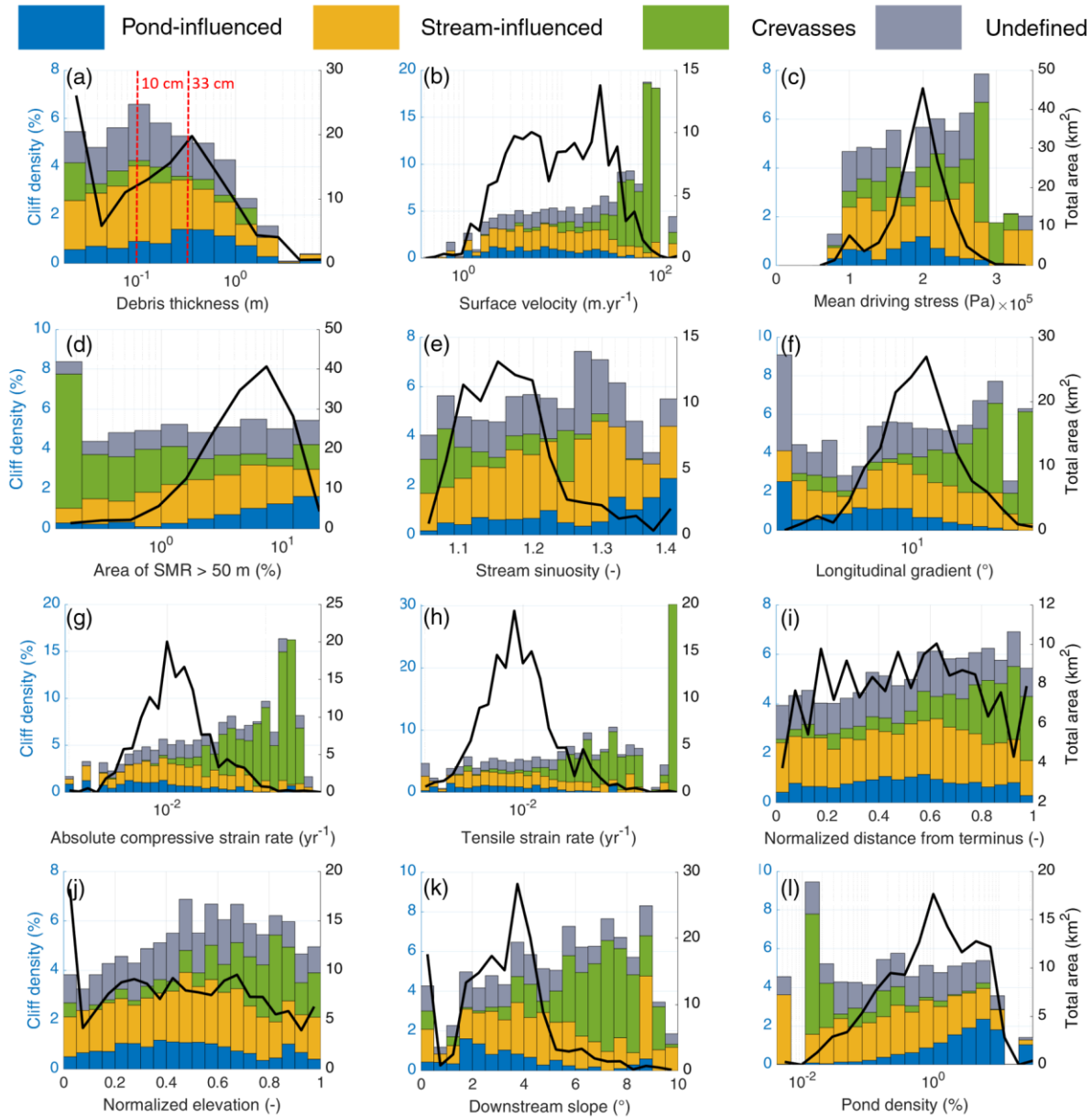
181  
 182 **Figure 2:** Cliff density for all glaciers as a function of (a) distance from ponds after  
 183 removal of the crevasses and (b) distance from streams, after removal of the pond-influenced  
 184 cliffs. The box plots indicate the median, 25th and 75th percentiles of the cliff density within each  
 185 10m bin for each glacier. The red dotted lines show the 40m buffers. (c) Area proportion of  
 186 undefined, pond- and stream-influenced cliffs and crevasses across all debris-covered glaciers.  
 187 (d) Pond density for all glaciers as a function of distance from cliffs. (h) Example of  
 188 classification of ice cliffs from Kyzylsu Glacier, Tajikistan: 1/ crevassed-areas, 2/ pond-  
 189 influenced cliffs and 3/ stream-influenced cliffs, with the pictures (e-g) and Pléiades view (i-k) of  
 190 the corresponding zones. Image credit: Marin Kneib and Evan S. Miles. Background of (i-k) is  
 191 the Pléiades false-colour multispectral image (19/09/2021). Pléiades © CNES 2021, Distribution  
 192 AIRBUS DS.

### 193 **3.2. Controls on ice cliff distribution**

194

195 The variables associated with ice cliff distribution vary depending on the category of cliff  
196 considered (Fig. 3, S15, Table S5). Stream-influenced and undefined cliffs follow a similar  
197 distribution for all predictors (Fig. S15), which could indicate that a majority of the undefined  
198 cliffs were formerly stream-influenced and backwasted away from the channels. 80% of stream-  
199 influenced cliffs are located in areas with debris estimated to be thinner than 33 cm, while 45%  
200 of the pond-influenced cliffs are located in areas with thicker debris (Fig. S15). This results in  
201 the total cliff density decreasing exponentially ( $Y = 5.8e^{-\frac{x}{2}}$ ,  $R^2 = 0.73$ ) when debris gets thicker  
202 than 10 cm (Fig. 3a, S16). Furthermore, crevasses and pond-influenced cliffs have a clearly  
203 contrasting response to the different controls investigated. Indeed, 80% of the crevasses are  
204 located in areas with surface velocities higher than the 13 m.yr<sup>-1</sup> threshold or in areas with debris  
205 thinner than 20 cm (Fig. S15). Pond-influenced cliffs clearly depend on pond density, and are  
206 thus preferentially located in non-dynamic areas with lower longitudinal gradient and velocity  
207 and with thicker debris (Fig. 3, S15, S17).

208



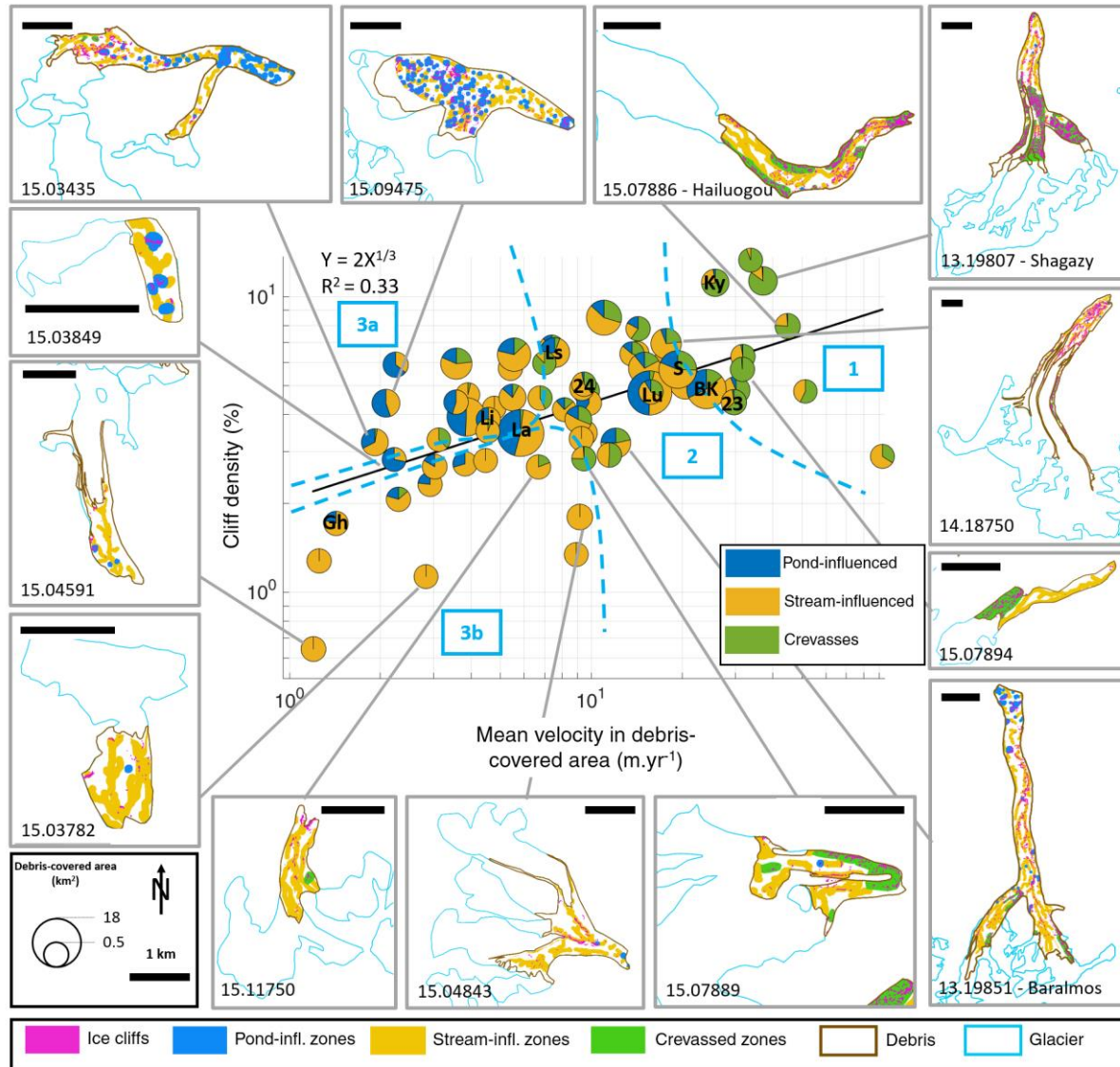
209  
 210 **Figure 3:** Mean cliff density split by cliff category for all bins of all glaciers where more than  
 211 65% of the debris-covered area could be classified as a function of (a) debris thickness, (b)  
 212 surface velocity, (c) mean driving stress, (d) ‘hummockiness’, (e) stream sinuosity, (f)  
 213 longitudinal gradient, (g) absolute compressive strain rate, (h) tensile strain rate, (i) normalized  
 214 distance from terminus, (j) normalized elevation above terminus, (k) downstream slope to  
 215 terminus and (l) pond density. The black line shows the area distribution of all the bins.

**3.2. Ice cliff dependence on glacier state**

218

219       When aggregating the metrics per glacier, a clear relationship between mean surface  
220 velocity across the debris-covered area and cliff density becomes apparent (Fig. 4, S18). The  
221 influence of climatic variables seems instead to be limited (Fig. S19). Cliff density decreases  
222 with decreasing velocity, up to a point where the trajectory seems to bifurcate. The debris-  
223 covered tongues with the highest cliff density and fastest velocity have a larger proportion of  
224 crevasses (state 1, Fig. 4). At slower velocities ( $<10 \text{ m.yr}^{-1}$ ), two trajectories are apparent: 1)  
225 glaciers with a large proportion ( $> \frac{1}{3}$ ) of pond-influenced cliffs and higher cliff densities (state  
226 3a, Fig 4), and 2) glaciers with a majority of stream-influenced cliffs, which tend to have lower  
227 cliff densities (state 3b, Fig. 4). The majority of the glaciers are found at an intermediary stage  
228 between these three end-members, with a decreasing proportion of crevasses and an increasing  
229 proportion of stream- and pond-influenced cliffs as velocity decreases (state 2, Fig. 4).

230



231  
 232 **Figure 4:** Glacier-wide cliff density as a function of mean velocity in the debris-covered  
 233 area for all glaciers where more than 65% of the debris-covered area could be classified. The  
 234 proportion of undefined cliffs was not represented for readability. The boxes to the side show  
 235 example maps of some of the glaciers with their surface classifications. Some additional  
 236 reference glaciers are indicated in the main plot in black. The expression and  $R^2$  of the black  
 237 linear regression are indicated in the upper left corner. In light blue are shown four glacier  
 238 clusters.

## 239 **4 Discussion and conclusions**

240 We have identified the presence of supraglacial streams and ponds, along with the  
241 opening of crevasses, to be the main mechanisms responsible for ice cliff formation and  
242 development. Newly-formed cliffs tend to be smaller in size and do not have any preferential  
243 aspect (Kneib et al., 2021; Fig. S4, S5). Cliffs get reburied when they backwaste away from  
244 these supraglacial features (Fig. 2a, b), with the strong control of solar radiation on cliff survival  
245 resulting in the preferentially poleward orientation of the total ice cliff population (Buri &  
246 Pellicciotti, 2018).

247

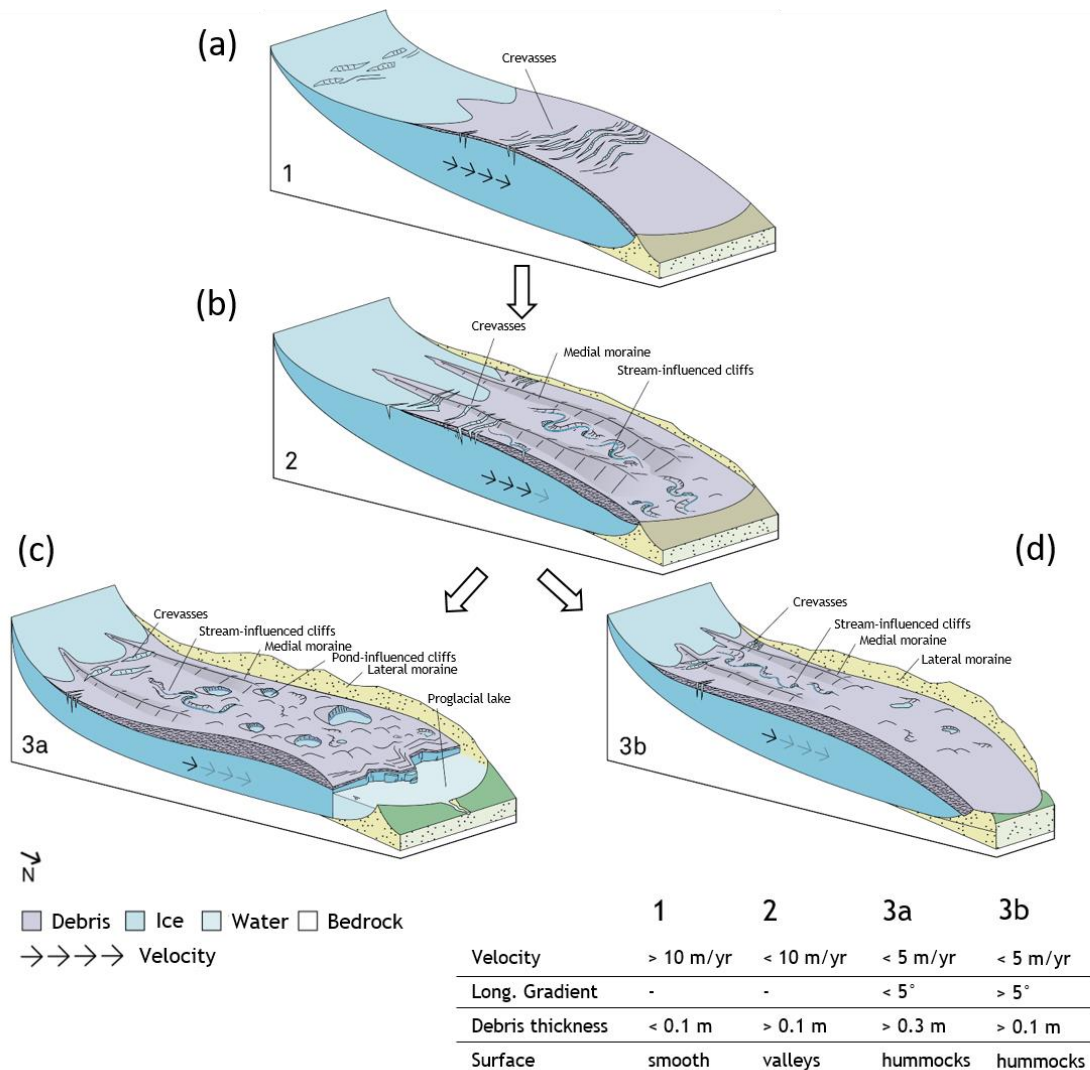
### 248 **4.1. Ice cliff distribution and glacier state**

249

250 Velocity stands out as the main control on ice cliff density both at the local and glacier  
251 scale (Fig. 3, 4). Interlinkages with other variables means that the cliff density also responds to  
252 other local controls, and debris thickness especially, although each category of cliffs responds  
253 differently (Fig. 3). The distribution of ice cliffs therefore depends on the glacier dynamics and  
254 state. A dynamic debris-covered glacier (mean surface velocity  $> 10 \text{ m.yr}^{-1}$ , Fig. 4, 5a, S20a) is  
255 usually characterised by thin debris and crevasses which comprise the majority of exposed ice  
256 and drain supraglacial streams. Glacier slow-down results in reduced strain rates and the  
257 migration of crevasses to the upper sections of the debris-covered area and their eventual  
258 disappearance (Fig. 3j, S20b), the extension of stream-influenced cliffs through debris  
259 destabilisation and thermo-erosional undercutting (Moore, 2018; Fig. 3a) and possibly the  
260 emergence of pond-influenced cliffs. Ponds maintain cliffs in more stagnant zones of thicker  
261 debris, also characterised by low longitudinal gradients and driving stress as well as increased  
262 hummock prevalence (Benn et al., 2017; Steiner et al., 2019; Watson, Quincey, Carrivick, et al.,  
263 2017; Fig. 5c). Such evolution has been observed on other glaciers: on Zmutt Glacier, where it  
264 was linked to the development of supraglacial valleys driven by stream incision (Mölg et al.,  
265 2020); and on Khumbu Glacier, where high relief zones characterised by growing cliffs and  
266 ponds have developed as the glacier has slowed (King et al., 2020; Rowan et al., 2021). Our  
267 large dataset enables us to show that this evolution holds across a large number of glaciers, and  
268 to identify predictors of cliff type and distribution. The development of large pond-influenced

269 cliffs however requires the accumulation of water in surface depressions, which occurs for larger  
 270 glaciers with lower longitudinal gradients (Fig. 4, 5c, S17). Most HMA glaciers in this stage of  
 271 evolution are located in the Central and Eastern Himalaya (Benn et al., 2012, 2017; Racoviteanu  
 272 et al., 2021; Watson et al., 2016; Watson, Quincey, Carrivick, et al., 2017; Fig. 1). However,  
 273 some glaciers do not develop such drainage systems due to their relative steepness and small  
 274 size, resulting in lower ice cliff densities (Fig. 4, 5d, S20d).

275  
 276



277  
 278 **Figure 5:** The four glacier evolution states, with their ice cliff distributions. State 1: fast  
 279 flowing glacier with thin debris and extensive crevassing. State 2: advanced debris cover, with  
 280 thicker debris and lower velocities enabling the development of supraglacial valleys and stream-

281 *influenced cliffs in the non-crevassed areas. State 3a: large stagnating debris-covered tongues,*  
282 *characterised by hummocks, thick debris and ponds maintaining cliffs in these zones. State 3b:*  
283 *stagnating tongues with thick debris, but high enough longitudinal gradient or low enough*  
284 *surface meltwater to prevent the formation of ponds and therefore the survival of cliffs. Figure*  
285 *credit: Martin Heynen.*

286

## 287 **4.2. Implications for glacier mass balance**

288

289 We have shown that ice cliff density and characteristics depend on the evolution state of the  
290 debris-covered glacier (Fig. 5), which is controlled mainly by dynamics (velocity) and debris  
291 thickness. Leveraging this new understanding of how glacier stage affects the presence of cliffs  
292 on their surfaces, we have provided the distribution of each type of cliff on glaciers at different  
293 stages of evolution (Fig. 3, 4, S20, Table S5). Future efforts should focus on testing the  
294 framework developed here by substantially expanding the number of data points with particular  
295 attention to include glaciers at distinct stages. Most of the debris-covered glaciers that have been  
296 the object of detailed investigations belong to glacier states 2 and 3 and efforts should be made  
297 to explore the whole range of evolution when targeting field studies. Already at this stage,  
298 however, the relationships detailed in this study outline a framework to estimate ice cliff  
299 distribution based on glacier flow characteristics, that are usually available in prognostic flow  
300 models, and debris thickness, without having to map the cliffs. Combined with cliff melt  
301 enhancement factors (E. S. Miles et al., 2022), this would allow long term estimation of the  
302 contribution of ice cliffs to debris-covered glacier mass balance - representing a key modelling  
303 advance.

304

305 Future work should also target the contribution of crevasses to glacier mass balance. Indeed,  
306 these features would likely enhance melt even more than traditional stream- and pond-influenced  
307 cliffs due to greater surface roughness at their location increasing turbulent fluxes, and additional  
308 reflected shortwave contributions from the opposite crevasse walls (Cathles et al., 2011; Colgan  
309 et al., 2016; W. T. Pfeffer & Bretherton, 1987; Purdie et al., 2022). Time-lapse images actually  
310 show the upper walls of crevasses backwasting as traditional ice cliffs would (Fig. S21).

311 Furthermore, their longer-term evolution and influence on shaping the debris-covered glacier  
312 surface remains unclear (Kirkbride & Deline, 2013).

313  
314

### 315 **Acknowledgments**

316 This project has received funding from the European Research Council (ERC) under the  
317 European Union's Horizon 2020 programme (grant agreement 772751) and from the Royal  
318 Society via a Newton Advanced Fellowship award (NA170325). The majority of the Pléiades  
319 stereo-pairs were provided by Etienne Berthier via the Pléiades Glacier Observatory (PGO)  
320 initiative of the French Space Agency (CNES). The remaining images were acquired through the  
321 CNES ISIS Programme. We thank the team of the Centre for Research on Glaciers at the  
322 Academy of Sciences of Tajikistan who enabled our 2021 fieldwork on Kyzylsu Glacier.

323

### 324 **Open Research**

325 The glacier, debris, crevasse, cliff and pond outlines will be made available on Zenodo. Other  
326 datasets used include surface velocity from Millan et al. (2022), climate data from ERA5-Land  
327 (Muñoz Sabater, 2019), RGI 6.0. glacier outlines (<https://nsidc.org/data/nsidc-0770/versions/6>), the  
328 AW3D 30m DEM (Tadono et al., 2014) and ice thicknesses (Farinotti et al., 2019). Atmospherically-  
329 corrected Sentinel-2 images prior to 2019 were obtained from CNES through the PEPS platform  
330 (Hagolle et al., 2015). From 2019 and later they were processed directly in Google Earth Engine.

331

### 332 **References**

333

334 Anderson, L. S., Armstrong, W. H., Anderson, R. S., & Buri, P. (2021). Debris cover and the  
335 thinning of Kennicott Glacier, Alaska: In situ measurements, automated ice cliff delineation  
336 and distributed melt estimates. *Cryosphere*, 15(1), 265–282. [https://doi.org/10.5194/tc-15-](https://doi.org/10.5194/tc-15-265-2021)  
337 265-2021

338 Anderson, L. S., Armstrong, W. H., Anderson, R. S., Scherler, D., & Petersen, E. (2021). The  
339 Causes of Debris-Covered Glacier Thinning: Evidence for the Importance of Ice Dynamics

- 340 From Kennicott Glacier, Alaska. *Frontiers in Earth Science*, 0, 723.  
341 <https://doi.org/10.3389/FEART.2021.680995>
- 342 Bartlett, O. T., Ng, F. S. L., & Rowan, A. V. (2020). Morphology and evolution of supraglacial  
343 hummocks on debris-covered Himalayan glaciers. *Earth Surface Processes and Landforms*,  
344 esp.5043. <https://doi.org/10.1002/esp.5043>
- 345 Benn, D. I., Wiseman, S., & Hands, K. A. (2001). Growth and drainage of supraglacial lakes on  
346 debris-mantled Ngozumpa Glacier, Khumbu Himal, Nepal. *Journal of Glaciology*, 47(159),  
347 626–638. <https://doi.org/10.3189/172756501781831729>
- 348 Benn, D. I., Bolch, T., Hands, K., Gulley, J., Luckman, A., Nicholson, L. I., et al. (2012,  
349 August). Response of debris-covered glaciers in the Mount Everest region to recent  
350 warming, and implications for outburst flood hazards. *Earth-Science Reviews*.  
351 <https://doi.org/10.1016/j.earscirev.2012.03.008>
- 352 Benn, Douglas I, Thompson, S., Gulley, J., Mertes, J., Luckman, A., & Nicholson, L. (2017).  
353 Structure and evolution of the drainage system of a Himalayan debris-covered glacier, and  
354 its relationship with patterns of mass loss. *The Cryosphere*, 11. [https://doi.org/10.5194/tc-](https://doi.org/10.5194/tc-11-2247-2017)  
355 [11-2247-2017](https://doi.org/10.5194/tc-11-2247-2017)
- 356 Berthier, E., Vincent, C., Magnússon, E., Gunnlaugsson, Á. Þ., Pitte, P., Le Meur, E., et al.  
357 (2014). Glacier topography and elevation changes derived from Pléiades sub-meter stereo  
358 images. *The Cryosphere*, 8, 2275–2291. <https://doi.org/10.5194/tc-8-2275-2014>
- 359 Bolch, T., Buchroithner, M. F., Peters, J., Baessler, M., & Bajracharya, S. (2008). Identification  
360 of glacier motion and potentially dangerous glacial lakes in the Mt. Everest region/Nepal  
361 using spaceborne imagery. *Natural Hazards and Earth System Sciences*, 8(6), 1329–1340.  
362 <https://doi.org/10.5194/nhess-8-1329-2008>

- 363 Brun, F., Buri, P., Miles, E. S., Wagnon, P., Steiner, J., Berthier, E., et al. (2016). Quantifying  
364 volume loss from ice cliffs on debris-covered glaciers using high-resolution terrestrial and  
365 aerial photogrammetry. *Journal of Glaciology*. <https://doi.org/10.1017/jog.2016.54>
- 366 Brun, F., Wagnon, P., Berthier, E., Shea, J. M., Immerzeel, W. W., Kraaijenbrink, P. D. A., et al.  
367 (2018). Ice cliff contribution to the tongue-wide ablation of Changri Nup Glacier, Nepal,  
368 central Himalaya. *The Cryosphere*, *12*(11), 3439–3457. [https://doi.org/10.5194/tc-12-3439-](https://doi.org/10.5194/tc-12-3439-2018)  
369 2018
- 370 Buri, P., & Pellicciotti, F. (2018). Aspect controls the survival of ice cliffs on debris-covered  
371 glaciers. *Proceedings of the National Academy of Sciences*, *115*(17), 4369–4374.  
372 <https://doi.org/10.1073/pnas.1713892115>
- 373 Buri, P., Pellicciotti, F., Steiner, J. F., Miles, E. S., & Immerzeel, W. W. (2016). A grid-based  
374 model of backwasting of supraglacial ice cliffs on debris-covered glaciers. *Annals of*  
375 *Glaciology*, *57*(71), 199–211. <https://doi.org/10.3189/2016AoG71A059>
- 376 Buri, P., Miles, E. S., Steiner, J. F., Ragetti, S., & Pellicciotti, F. (2021). Supraglacial Ice Cliffs  
377 Can Substantially Increase the Mass Loss of Debris-Covered Glaciers. *Geophysical*  
378 *Research Letters*, *48*(6). <https://doi.org/10.1029/2020GL092150>
- 379 Cathles, L. M., Abbot, D. S., Bassis, J. N., & MacAyeal, D. R. (2011). Modeling surface-  
380 roughness/solar-ablation feedback: application to small-scale surface channels and  
381 crevasses of the Greenland ice sheet. *Annals of Glaciology*, *52*(59), 99–108.  
382 <https://doi.org/10.3189/172756411799096268>
- 383 Colgan, W., Rajaram, H., Abdalati, W., McCutchan, C., Mottram, R., Moussavi, M. S., &  
384 Grigsby, S. (2016, March 1). Glacier crevasses: Observations, models, and mass balance  
385 implications. *Reviews of Geophysics*. Blackwell Publishing Ltd.

- 386 <https://doi.org/10.1002/2015RG000504>
- 387 Compagno, L., Huss, M., Miles, E. S., McCarthy, M. J., Zekollari, H., Dehecq, A., et al. (2022).  
388 Modelling supraglacial debris-cover evolution from the single-glacier to the regional scale:  
389 an application to High Mountain Asia. *The Cryosphere*, *16*(5), 1697–1718.  
390 <https://doi.org/10.5194/tc-16-1697-2022>
- 391 Dehecq, A., Gourmelen, N., Gardner, A. S., Brun, F., Goldberg, D., Nienow, P. W., et al. (2019).  
392 Twenty-first century glacier slowdown driven by mass loss in High Mountain Asia. *Nature*  
393 *Geoscience*, *12*(1), 22–27. <https://doi.org/10.1038/s41561-018-0271-9>
- 394 Egli, P. E., Belotti, B., Ouvry, B., Irving, J., & Lane, S. N. (2021). Subglacial Channels, Climate  
395 Warming, and Increasing Frequency of Alpine Glacier Snout Collapse. *Geophysical*  
396 *Research Letters*, *48*(21). <https://doi.org/10.1029/2021GL096031>
- 397 Falaschi, D., Rivera, A., Lo Vecchio Repetto, A., Moragues, S., Villalba, R., Rastner, P., et al.  
398 (2021). Evolution of Surface Characteristics of Three Debris-Covered Glaciers in the  
399 Patagonian Andes From 1958 to 2020. *Frontiers in Earth Science*, *9*.  
400 <https://doi.org/10.3389/feart.2021.671854>
- 401 Farinotti, D., Huss, M., Fürst, J. J., Landmann, J., Machguth, H., Maussion, F., & Pandit, A.  
402 (2019). A consensus estimate for the ice thickness distribution of all glaciers on Earth.  
403 *Nature Geoscience*, *12*(3), 168–173. <https://doi.org/10.1038/s41561-019-0300-3>
- 404 Ferguson, J. C., & Vieli, A. (2021). Modelling steady states and the transient response of debris-  
405 covered glaciers. *The Cryosphere*, *15*(7), 3377–3399. [https://doi.org/10.5194/tc-15-3377-](https://doi.org/10.5194/tc-15-3377-2021)  
406 [2021](https://doi.org/10.5194/tc-15-3377-2021)
- 407 Gulley, J. D., Benn, D. I., Screatton, E., & Martin, J. (2009). Mechanisms of englacial conduit  
408 formation and their implications for subglacial recharge. *Quaternary Science Reviews*,

- 409 28(19–20), 1984–1999. <https://doi.org/10.1016/j.quascirev.2009.04.002>
- 410 Hagolle, O., Huc, M., Villa Pascual, D., & Dedieu, G. (2015). A Multi-Temporal and Multi-  
411 Spectral Method to Estimate Aerosol Optical Thickness over Land, for the Atmospheric  
412 Correction of FormoSat-2, LandSat, VEN $\mu$ S and Sentinel-2 Images. *Remote Sensing*, 7(3),  
413 2668–2691. <https://doi.org/10.3390/rs70302668>
- 414 Herreid, S., & Pellicciotti, F. (2018). Automated detection of ice cliffs within supraglacial debris  
415 cover. *The Cryosphere*, 12, 1811–1829. <https://doi.org/10.5194/tc-12-1811-2018>
- 416 Herreid, S., & Pellicciotti, F. (2020). The state of rock debris covering Earth’s glaciers. *Nature*  
417 *Geoscience*, 1–7. <https://doi.org/10.1038/s41561-020-0615-0>
- 418 Immerzeel, W. W., Kraaijenbrink, P. D. A., Shea, J. M., Shrestha, A. B., Pellicciotti, F.,  
419 Bierkens, M. F. P., & De Jong, S. M. (2014). High-resolution monitoring of Himalayan  
420 glacier dynamics using unmanned aerial vehicles. *Remote Sensing of Environment*, 150, 93–  
421 103. <https://doi.org/10.1016/j.rse.2014.04.025>
- 422 Kienholz, C., Rich, J. L., Arendt, A. A., & Hock, R. (2014). A new method for deriving glacier  
423 centerlines applied to glaciers in Alaska and northwest Canada. *The Cryosphere*, 8(2), 503–  
424 519. <https://doi.org/10.5194/tc-8-503-2014>
- 425 King, O., Turner, A. G. D., Quincey, D. J., & Carrivick, J. L. (2020). Morphometric evolution of  
426 Everest region debris-covered glaciers. *Geomorphology*, 371, 107422.  
427 <https://doi.org/10.1016/j.geomorph.2020.107422>
- 428 Kirkbride, M. P., & Deline, P. (2013). The formation of supraglacial debris covers by primary  
429 dispersal from transverse englacial debris bands. *Earth Surface Processes and Landforms*,  
430 38(15), 1779–1792. <https://doi.org/10.1002/esp.3416>
- 431 Kneib, M., Miles, E. S., Jola, S., Buri, P., Herreid, S., Bhattacharya, A., et al. (2020). Mapping

- 432 ice cliffs on debris-covered glaciers using multispectral satellite images. *Remote Sensing of*  
433 *Environment*, 112201. <https://doi.org/10.1016/j.rse.2020.112201>
- 434 Kneib, M., Miles, E. S., Buri, P., Molnar, P., McCarthy, M., Fugger, S., & Pellicciotti, F. (2021).  
435 Interannual Dynamics of Ice Cliff Populations on Debris-Covered Glaciers From Remote  
436 Sensing Observations and Stochastic Modeling. *Journal of Geophysical Research: Earth*  
437 *Surface*, 126(10). <https://doi.org/10.1029/2021JF006179>
- 438 Kneib, Marin, Miles, E. S., Buri, P., Fugger, S., McCarthy, M., Shaw, T. E., et al. (2022). Sub-  
439 seasonal variability of supraglacial ice cliff melt rates and associated processes from time-  
440 lapse photogrammetry. *The Cryosphere*, 16(11), 4701–4725. [https://doi.org/10.5194/tc-16-](https://doi.org/10.5194/tc-16-4701-2022)  
441 [4701-2022](https://doi.org/10.5194/tc-16-4701-2022)
- 442 Kraaijenbrink, P. D. A., Shea, J. M., Pellicciotti, F., De Jong, S. M., & Immerzeel, W. W.  
443 (2016). Object-based analysis of unmanned aerial vehicle imagery to map and characterise  
444 surface features on a debris-covered glacier. *Remote Sensing of Environment*, 186, 581–595.  
445 <https://doi.org/10.1016/j.rse.2016.09.013>
- 446 Loriaux, T., & Ruiz, L. (2021). Spatio-Temporal Distribution of Supra-Glacial Ponds and Ice  
447 Cliffs on Verde Glacier, Chile. *Frontiers in Earth Science*, 9.  
448 <https://doi.org/10.3389/feart.2021.681071>
- 449 McCarthy, M., Miles, E., Kneib, M., Buri, P., Fugger, S., & Pellicciotti, F. (2022). Supraglacial  
450 debris thickness and supply rate in High-Mountain Asia. *Communications Earth &*  
451 *Environment*, 3(1), 269. <https://doi.org/10.1038/s43247-022-00588-2>
- 452 McFeeters, S. K. (1996). The use of the Normalized Difference Water Index (NDWI) in the  
453 delineation of open water features. *International Journal of Remote Sensing*, 17(7), 1425–  
454 1432. <https://doi.org/10.1080/01431169608948714>

- 455 Miles, E. S., Willis, I. C., Arnold, N. S., Steiner, J., & Pellicciotti, F. (2017). Spatial, seasonal  
456 and interannual variability of supraglacial ponds in the Langtang Valley of Nepal, 1999-  
457 2013. <https://doi.org/10.1017/jog.2016.120>
- 458 Miles, E. S., Watson, C. S., Brun, F., Berthier, E., Esteves, M., Quincey, D. J., et al. (2018).  
459 Glacial and geomorphic effects of a supraglacial lake drainage and outburst event, Everest  
460 region, Nepal Himalaya. *The Cryosphere*, 12, 3891–3905. [https://doi.org/10.5194/tc-12-](https://doi.org/10.5194/tc-12-3891-2018)  
461 3891-2018
- 462 Miles, E. S., Willis, I., Buri, P., Steiner, J. F., Arnold, N. S., & Pellicciotti, F. (2018). Surface  
463 Pond Energy Absorption Across Four Himalayan Glaciers Accounts for 1/8 of Total  
464 Catchment Ice Loss. *Geophysical Research Letters*, 45(19), 10,464-10,473.  
465 <https://doi.org/10.1029/2018GL079678>
- 466 Miles, E. S., Steiner, J. F., Buri, P., Immerzeel, W. W., & Pellicciotti, F. (2022). Controls on the  
467 relative melt rates of debris-covered glacier surfaces. *Environmental Research Letters*,  
468 17(6), 064004. <https://doi.org/10.1088/1748-9326/ac6966>
- 469 Miles, K. E., Hubbard, B., Irvine-Fynn, T. D. L., Miles, E., Quincey, D. J., & Rowan, A. V.  
470 (2020, August 1). Hydrology of debris-covered glaciers in High Mountain Asia. *Earth-*  
471 *Science Reviews*. Elsevier B.V. <https://doi.org/10.1016/j.earscirev.2020.103212>
- 472 Millan, R., Mouginot, J., Rabatel, A., & Morlighem, M. (2022). Ice velocity and thickness of the  
473 world's glaciers. *Nature Geoscience*, 15(2), 124–129. [https://doi.org/10.1038/s41561-021-](https://doi.org/10.1038/s41561-021-00885-z)  
474 00885-z
- 475 Mölg, N., Bolch, T., Walter, A., & Vieli, A. (2019). Unravelling the evolution of Zmuttgletscher  
476 and its debris cover since the end of the Little Ice Age. *The Cryosphere*, 13(7), 1889–1909.  
477 <https://doi.org/10.5194/tc-13-1889-2019>

- 478 Mölg, N., Ferguson, J., Bolch, T., & Vieli, A. (2020). On the influence of debris cover on glacier  
479 morphology: How high-relief structures evolve from smooth surfaces. *Geomorphology*,  
480 357, 107092. <https://doi.org/10.1016/j.geomorph.2020.107092>
- 481 Moore, P. L. (2018). Stability of supraglacial debris. *Earth Surface Processes and Landforms*,  
482 43(1), 285–297. <https://doi.org/10.1002/esp.4244>
- 483 Moore, P. L. (2021). Numerical Simulation of Supraglacial Debris Mobility: Implications for  
484 Ablation and Landform Genesis. *Frontiers in Earth Science*, 9.  
485 <https://doi.org/10.3389/feart.2021.710131>
- 486 Muñoz Sabater, J. (2019). ERA5-Land monthly averaged data from 1981 to present. *Copernicus*  
487 *Climate Change Service (C3S) Climate Data Store (CDS)*.  
488 <https://doi.org/10.24381/cds.68d2bb30>
- 489 Nicholson, L. I., McCarthy, M., Pritchard, H. D., & Willis, I. (2018). Supraglacial debris  
490 thickness variability: Impact on ablation and relation to terrain properties. *Cryosphere*,  
491 12(12), 3719–3734. <https://doi.org/10.5194/tc-12-3719-2018>
- 492 Pellicciotti, F., Stephan, C., Miles, E. S., Herreid, S., Immerzeel, W. W., & Bolch, T. (2015).  
493 Mass-balance changes of the debris-covered glaciers in the Langtang Himal, Nepal, from  
494 1974 to 1999. *Journal of Glaciology*, 61(226), 373–386.  
495 <https://doi.org/10.3189/2015JoG13J237>
- 496 Pfeffer, W. T., & Bretherton, C. S. (1987). The effect of crevasses on the solar heating of a  
497 glacier surface. *The Physical Basis of Ice Sheet Modelling*, 170, 191–205.
- 498 Pfeffer, W. T., Arendt, A. A., Bliss, A., Bolch, T., Cogley, J. G., Gardner, A. S., et al. (2014).  
499 The Randolph glacier inventory: A globally complete inventory of glaciers. *Journal of*  
500 *Glaciology*, 60(221), 537–552. <https://doi.org/10.3189/2014JoG13J176>

- 501 Purdie, H., Zawar-Reza, P., Katurji, M., Schumacher, B., Kerr, T., & Bealing, P. (2022).  
502 Variability in the vertical temperature profile within crevasses at an alpine glacier. *Journal*  
503 *of Glaciology*, 1–15. <https://doi.org/10.1017/jog.2022.73>
- 504 Quincey, D. J., & Glasser, N. F. (2009). Morphological and ice-dynamical changes on the  
505 Tasman Glacier, New Zealand, 1990–2007. *Global and Planetary Change*, 68(3), 185–197.  
506 <https://doi.org/10.1016/j.gloplacha.2009.05.003>
- 507 Quincey, D. J., Richardson, S. D., Luckman, A., Lucas, R. M., Reynolds, J. M., Hambrey, M. J.,  
508 & Glasser, N. F. (2007). Early recognition of glacial lake hazards in the Himalaya using  
509 remote sensing datasets. *Global and Planetary Change*, 56(1–2), 137–152.  
510 <https://doi.org/10.1016/j.gloplacha.2006.07.013>
- 511 Racoviteanu, A. E., Nicholson, L., & Glasser, N. F. (2021). Surface composition of debris-  
512 covered glaciers across the Himalaya using linear spectral unmixing of Landsat 8 OLI  
513 imagery. *The Cryosphere*, 15, 4557–4588. <https://doi.org/10.5194/tc-15-4557-2021>
- 514 Racoviteanu, A. E., Glasser, N. F., Robson, B. A., Harrison, S., Millan, R., Kayastha, R. B., &  
515 Kayastha, R. (2022). Recent Evolution of Glaciers in the Manaslu Region of Nepal From  
516 Satellite Imagery and UAV Data (1970–2019). *Frontiers in Earth Science*, 9.  
517 <https://doi.org/10.3389/feart.2021.767317>
- 518 Reid, T. D., & Brock, B. W. (2014). Assessing ice-cliff backwasting and its contribution to total  
519 ablation of debris-covered Miage glacier, Mont Blanc massif, Italy. *Journal of Glaciology*.  
520 <https://doi.org/10.3189/2014JoG13J045>
- 521 Reynolds, J. (2000). On the formation of supraglacial lakes on debris-covered glaciers. *IAHS-*  
522 *AISH Publication*, 264, 153–161.
- 523 Röhl, K. (2006). Thermo-erosional notch development at fresh-water-calving Tasman Glacier,

- 524 New Zealand. *Journal of Glaciology*, 52(177), 203–213.  
525 <https://doi.org/10.3189/172756506781828773>
- 526 Röhl, K. (2008). Characteristics and evolution of supraglacial ponds on debris-covered Tasman  
527 Glacier, New Zealand. *Journal of Glaciology*.  
528 <https://doi.org/10.3189/002214308787779861>
- 529 Rounce, D. R., Hock, R., McNabb, R. W., Millan, R., Sommer, C., Braun, M. H., et al. (2021).  
530 Distributed global debris thickness estimates reveal debris significantly impacts glacier  
531 mass balance. *Geophysical Research Letters*, e2020GL091311.  
532 <https://doi.org/10.1029/2020GL091311>
- 533 Rowan, A. V., Egholm, D. L., Quincey, D. J., Hubbard, B., King, O., Miles, E. S., et al. (2021).  
534 The Role of Differential Ablation and Dynamic Detachment in Driving Accelerating Mass  
535 Loss From a Debris-Covered Himalayan Glacier. *Journal of Geophysical Research: Earth*  
536 *Surface*, 126(9), e2020JF005761. <https://doi.org/10.1029/2020JF005761>
- 537 Sakai, A., & Fujita, K. (2010). Formation conditions of supraglacial lakes on debris-covered  
538 glaciers in the Himalaya. *Journal of Glaciology*, 56(195), 177–181.  
539 <https://doi.org/10.3189/002214310791190785>
- 540 Sakai, A., & Takeuchi, N. (2000). *Debris-Covered Glaciers*. IAHS Publ.
- 541 Sakai, A., Nakawo, M., & Fujita, K. (1998). Melt rate of ice cliffs on the Lirung Glacier, Nepal  
542 Himalayas, 1996. *Bulletin of Glacier Research*, 16, 57–66.
- 543 Sakai, A., Nakawo, M., & Fujita, K. (2002). Distribution Characteristics and Energy Balance of  
544 Ice Cliffs on Debris-covered Glaciers, Nepal Himalaya. *Arctic, Antarctic, and Alpine*  
545 *Research*, 34(1), 12–19. <https://doi.org/10.1080/15230430.2002.12003463>
- 546 Salerno, F., Thakuri, S., D'Agata, C., Smiraglia, C., Manfredi, E. C., Viviano, G., & Tartari, G.

- 547 (2012). Glacial lake distribution in the Mount Everest region: Uncertainty of measurement  
548 and conditions of formation. *Global and Planetary Change*, 92–93, 30–39.  
549 <https://doi.org/10.1016/j.gloplacha.2012.04.001>
- 550 Sato, Y., Fujita, K., Inoue, H., Sunako, S., Sakai, A., Tsushima, A., et al. (2021). Ice Cliff  
551 Dynamics of Debris-Covered Trakarding Glacier in the Rolwaling Region, Nepal Himalaya.  
552 *Frontiers in Earth Science*, 9, 398. <https://doi.org/10.3389/FEART.2021.623623/BIBTEX>
- 553 Scherler, D., Wulf, H., & Gorelick, N. (2018). Global Assessment of Supraglacial Debris-Cover  
554 Extents. *Geophysical Research Letters*. <https://doi.org/10.1029/2018GL080158>
- 555 Schwanghart, W., & Scherler, D. (2014). Short Communication: TopoToolbox 2 – MATLAB-  
556 based software for topographic analysis and modeling in Earth surface sciences. *Earth*  
557 *Surface Dynamics*, 2(1), 1–7. <https://doi.org/10.5194/esurf-2-1-2014>
- 558 Sharp, R. P. (1949). Studies of superglacial debris on valley glaciers. *American Journal of*  
559 *Science*, 247(5), 289–315. <https://doi.org/10.2475/ajs.247.5.289>
- 560 Shean, D. E., Alexandrov, O., Moratto, Z. M., Smith, B. E., Joughin, I. R., Porter, C., & Morin,  
561 P. (2016). An automated, open-source pipeline for mass production of digital elevation  
562 models (DEMs) from very-high-resolution commercial stereo satellite imagery. *ISPRS*  
563 *Journal of Photogrammetry and Remote Sensing*, 116, 101–117.  
564 <https://doi.org/10.1016/j.isprsjprs.2016.03.012>
- 565 Steiner, J. F., Buri, P., Miles, E. S., Ragetti, S., & Pellicciotti, F. (2019). Supraglacial ice cliffs  
566 and ponds on debris-covered glaciers: Spatio-temporal distribution and characteristics.  
567 *Journal of Glaciology*, 65(252), 617–632. <https://doi.org/10.1017/jog.2019.40>
- 568 Stokes, C. R., Popovnin, V., Aleynikov, A., Gurney, S. D., & Shahgedanova, M. (2007). Recent  
569 glacier retreat in the Caucasus Mountains, Russia, and associated increase in supraglacial

570 debris cover and supra-/proglacial lake development. In *Annals of Glaciology* (Vol. 46, pp.  
571 195–203). <https://doi.org/10.3189/172756407782871468>

572 Tadono, T., Ishida, H., Oda, F., Naito, S., Minakawa, K., & Iwamoto, H. (2014). Precise Global  
573 DEM Generation by ALOS PRISM. *ISPRS Annals of the Photogrammetry, Remote Sensing  
574 and Spatial Information Sciences, II-4*, 71–76. [https://doi.org/10.5194/isprsannals-II-4-71-](https://doi.org/10.5194/isprsannals-II-4-71-2014)  
575 2014

576 Watson, C. S., Quincey, D. J., Carrivick, J. L., & Smith, M. W. (2016). The dynamics of  
577 supraglacial ponds in the Everest region, central Himalaya. *Global and Planetary Change*,  
578 *142*, 14–27. [https://doi.org/https://doi.org/10.1016/j.gloplacha.2016.04.008](https://doi.org/10.1016/j.gloplacha.2016.04.008)

579 Watson, C. S., Quincey, D. J., Carrivick, J. L., & Smith, M. W. (2017). Ice cliff dynamics in the  
580 Everest region of the Central Himalaya. *Geomorphology*, *278*, 238–251.  
581 <https://doi.org/10.1016/j.geomorph.2016.11.017>

582 Watson, C. S., Quincey, D. J., Smith, M. W., Carrivick, J. L., Rowan, A. V., & James, M. R.  
583 (2017). Quantifying ice cliff evolution with multi-temporal point clouds on the debris-  
584 covered Khumbu Glacier, Nepal. <https://doi.org/10.1017/jog.2017.47>

585 Watson, C. S., King, O., Miles, E. S., & Quincey, D. J. (2018). Optimising NDWI supraglacial  
586 pond classification on Himalayan debris-covered glaciers. *Remote Sensing of Environment*,  
587 *217*, 414–425. <https://doi.org/10.1016/j.rse.2018.08.020>

588

589

#### 590 **Additional references in supporting information**

591

592 Fugger, S., Fyffe, C.L., Fatichi, S., Miles, E., McCarthy, M., Shaw, T.E., Ding, B., Yang, W.,  
593 Wagon, P., Immerzeel, W., Liu, Q., Pellicciotti, F., 2022. Understanding monsoon controls

594 on the energy and mass balance of glaciers in the Central and Eastern Himalaya. *Cryosph.*  
595 16, 1631–1652. <https://doi.org/10.5194/tc-16-1631-2022>

596  
597  
598  
599